

Quantum effects and temperature dependence of the free energy barrier and shear frequency in bilayer graphene

Jean Paul Nery,^{1,2,*} Lorenzo Monacelli,¹ and Francesco Mauri^{1,2,†}

¹*Dipartimento di Fisica, Università di Roma La Sapienza, I-00185 Roma, Italy*

²*Graphene Labs, Fondazione Istituto Italiano di Tecnologia, Via Morego, I-16163 Genova, Italy*

Little is known about the quantum effects of friction, and first-principles studies are virtually non-existent. In multilayer graphene, the order of the stacking of the layers plays a crucial role in the electronic properties and the manifestation of superconductivity, and friction affects how layers slide to change the stacking. Here, we study the effects of friction in bilayer graphene by focusing on quantum fluctuations in the free energy barrier that layers have to overcome to slide with respect to each other. We evaluate the free energy at the barrier in bilayer graphene through the self-consistent harmonic approximation, accounting for quantum and thermal ionic fluctuations. We obtain a very large reduction of the barrier of more than 30%. Temperature effects are weaker, although high temperatures induce a significant reduction of the barrier as well. Our approach is general and paves the way for systematically accounting for nuclear quantum and thermal effects in free energy barriers of other macroscopic systems.

There has been intense research on graphene since its discovery in 2004, and also on multilayer graphene systems. Among many other interesting properties, flat bands are present in multilayer rhombohedral (ABC-stacked) graphene (RG)¹, and in fact, superconductivity has been observed in RG in 2021². Several works recently studied, both experimentally and theoretically, under which conditions RG can form³⁻⁸. In particular, some of us unveiled how the stacking of graphene layers changes under shear stress⁹, and obtained that it produces many consecutive layers of RG. In fact, all samples with long-range RG that have been observed so far have been subject to some form of shear stress^{5,10-14}, and thus of friction.

To move graphene layers with respect to each other, they have to overcome a free energy barrier that separates different minima. When doing so, they experiment “stick-slip” motion: they move gradually with increasing shear stress, followed by sudden rearrangements and decrease of the stress¹⁵. The maximum shear-stress to “unlock” layers is correlated with the height of the barrier. Such barrier corresponds to the activation energy of a metastable state, where a graphene flake (from nanometers up to possibly micrometer scales) sitting on top of a large graphene layer is displaced relative to the equilibrium position. In clean samples with micrometer sized flakes however, different regions can have different stackings (AB and AC)^{12,16}, and a domain wall in the metastable state separates both regions. The displacement of layers in this case is more complex and is not considered in our work.

Superlubricity is another phenomenon present in systems involving graphene layers or graphite that has attracted a lot of attention^{17,18}, in which the energy landscape corresponding to the relative displacement of graphene layers is also central. Some works have studied how quantum effects, including zero-point renormaliza-

tion (ZPR) and tunneling, affect the free-energy barrier of dissociative adsorption¹⁹ and diffusion²⁰⁻²² of hydrogen. However, there are no studies of the quantum effects and temperature dependence of free-energy barriers in macroscopic systems.

A quantity closely related to the free energy barrier is the shear frequency, corresponding to the mode in which layers move rigidly in-plane and out of phase around the equilibrium position. The free energy barrier separates two equivalent minima, so the barrier and shear frequency are expected to have a similar temperature dependence (a lower curvature at the minima corresponds to a lower shear frequency and a lower free energy, at least close to the minima). The value of the shear frequency in graphite is a relatively well-established quantity, with experimental values²³ oscillating between 42 - 45 cm⁻¹, using for example inelastic X-ray scattering²⁴, neutron-coherent inelastic scattering²⁵, Raman spectra^{26,27}, and coherent phonon spectroscopy²⁸. In bilayer graphene, there are some experiments with values around 30 cm⁻¹; for example, 28 ± 3 cm⁻¹ in Refs. 28 and 29, and 32 cm⁻¹ in Ref. 26. The temperature dependence of the shear modes, however, has been barely studied. Few experiments measure the temperature dependence of the shear mode, using Raman scattering in folded 2+2 (4 layer) graphene³⁰, or femtosecond pump-probe spectroscopy in graphite³¹.

Another aspect of multilayer graphene and graphite that still needs further investigation and that serves as a consistency check on the adequacy of our approach is thermal expansion (TE). Ref. 32 measured it in bilayer and trilayer graphene for the first time. Ref. 33 uses QHA, which underestimates the out-of-plane TE at low temperatures³⁴ and has a very rapid increase at high temperatures; in-plane, it also underestimates the TE at low temperatures³⁴ and overestimates it at high temperatures³⁵. Much better out-of-plane results

were obtained by using path integral molecular dynamics (PIMD)³⁶, but while the TE flattens at 500 K in graphite, experimental values continue increasing^{35,37}. However, in-plane PIMD results of Ref. 36 vastly overestimate the TE.

Motivated by the aforementioned phenomena, especially by the lack of understanding of quantum effects in friction, we focus on studying the ZPR and temperature effects of the free-energy barrier. This is a very challenging problem due to the difficulty of determining the free energy in a non-equilibrium position. Here we tackle it using the state-of-the-art stochastic self-consistent harmonic approximation (SSCHA)³⁸. First, we compare our results to the height of the barrier with fixed atoms. Then, using also the quasiharmonic approximation (QHA), we calculate the temperature dependence of the shear frequency and compare to the limited experimental data available. Finally, we determine the in-plane and out-of-plane TE coefficient in bilayer graphene and graphite, and compare our results to previous theoretical and experimental work.

We first focus on studying bilayer graphene, where the in-plane and (most importantly) out-of-plane interactions are given by the interatomic potential of Ref. 39 and Ref. 40, respectively. The out-of-plane interactions determine the barrier. The energy profile of a layer moving with respect to the other one along the bond direction is given by Fig. 1, which gives good results when comparing to theory and experiment (see Table I).

TABLE I. Comparison of the barrier V_{SP} and the shear frequency at fixed ionic positions (classical) between the interatomic potential we used in this work^{39,40}, LDA, and theoretical calculations and experiments from previous works. The values are a little bit lower but close to that of adiabatic-connection fluctuation-dissipation theorem within the random phase approximation (ACFDT-RPA)⁴¹ and experimental data²³.

	2 layers This work	2 layers LDA	Previous works
Small barrier V_{SP} (meV/atom)	1.24	1.58	1.53 (RPA) ⁴¹
Shear frequency (cm^{-1}) (bulk)	37	42	42-45 ²³

The lower layer is fixed in position A, and there are two minima of the same energy, AB and AC, at a distance of a bond length $d = 1.42$ Å. For layers to slide with respect to each other, they have to overcome a barrier V_{SP} . SP is a saddle point in the full energy landscape, so the shear mode in the perpendicular direction (along the direction of two nearby AA maxima) is stable. In order to determine the ZPR and temperature dependence of the barrier, we use SSCHA to determine

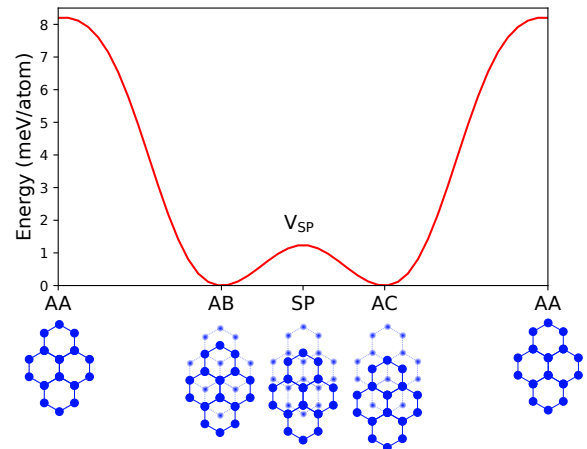


FIG. 1. Energy profile of bilayer graphene when moving one layer relative to the other along the bond direction. The lower layer is fixed in position A. Configuration AA (one layer on top of each other) is the least favorable configuration. There are two minima of the same energy, AB and AC, which correspond to the two stable configurations. To go from one minima to the other one applying shear stress, the upper layer has to overcome the barrier V_{SP} , which has a value of 1.24 meV/atom relative to the minima. The diagrams below illustrate the different configurations, with the upper layer (darker blue) moving relative to the lower one in position A (lighter blue).

the free energy at the equilibrium position and SP.

The SSCHA minimizes the quantum free energy similarly to a variational Monte Carlo for nuclei, optimizing an *ansatz* density matrix of the most general Gaussian. The average atomic positions of the layers can be constrained at SP, and thanks to the simple shape of the variational *ansatz*, a quantum-free energy can be rigorously defined^{38,42}. Notably, QHA cannot determine the barrier as the harmonic frequencies are not well-defined at SP. On the other hand, the SSCHA free energy landscape remains properly defined even in out-of-equilibrium and unstable configurations like SP. The Gaussian *ansatz* of the SSCHA allows separating the total free energy in an auxiliary harmonic contribution, which is long-ranged and can be interpolated up to a very fine k -mesh (40×40), fundamental to avoid oversampling the energy of the shear mode, and a short-range anharmonic contribution, which can be properly converged already with small simulation cells. More details about QHA, SSCHA, and the interpolation method can be found in the Appendix.

The barrier as a function of temperature can be seen in Fig. 2. The effects of the ZPR are very large: the barrier is reduced by an outstanding 35% with respect to the value at fixed nuclei. Since the frictional force is expected to be proportional to the barrier, quantum effects play a decisive role in the ability of layers to slide with respect to each other. Several other systems also

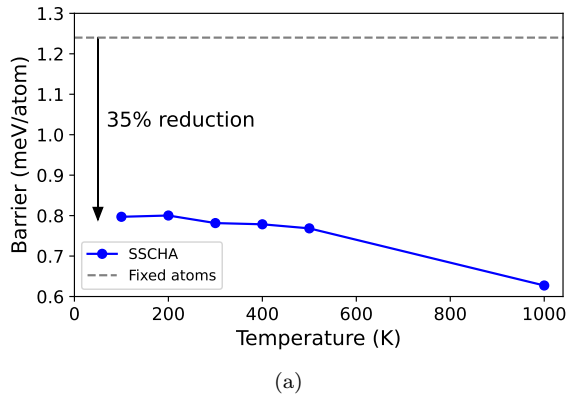


FIG. 2. Barrier as a function of temperature. It is reduced from 1.24 meV/atom, the value at fixed nuclei (V_{SP} in Fig. 1), to about 0.8 meV/atom, corresponding to a large ZPR of about 35%. The barrier does not change much up to about 500 K, but the value at 1000 K is about 20% smaller relative to the value at 100 K. The lines are a guide to the eye, as in the other figures of this work.

present a reduction (sometimes also substantial) of the free energy relative to classical values, like adsorption or diffusion of hydrogen on several materials^{19–22}. In terms of temperature effects, they are almost entirely covered by quantum fluctuations, since the barrier remains constant at around 0.8 meV/atom up to 500 K. Still when temperature increases up to 1000 K, the barrier is further reduced by 20% relative to the value at 100 K. Thus, high temperatures should help to reduce (static) friction between layers.

At the equilibrium position, one of the vibrational modes at Γ is the shear mode in both directions of the plane (doubly degenerate, see Fig. 3). Its temperature dependence can be determined using both SSCHA and QHA. In the QHA, the TE is obtained by determining the lattice parameters that minimize the free energy at each temperature. The harmonic phonon frequencies calculated at such lattice parameters then also give temperature dependent frequencies. See Appendix Sec. A1 a for more details. The third out of phase mode of the layers is the breathing mode, in the out-of-plane direction. A discussion of its temperature dependence can also be found in the Appendix.

The temperature dependence of the shear frequency can be seen in Fig. 4. The quantum effects evaluated within the SSCHA harden the shear frequency energy at low temperatures compared with the classical value at 0 K (dashed line). On the other hand, the ZPR in QHA softens the shear frequency. The temperature dependence of the shear mode is similar to the barrier, varying by about 20% from 0 to 1000 K, and having a larger dependence at temperatures above 500 K.

Regarding the experimental data, in Ref. 30, the measurements are done in 2+2 folded graphene (4 layers).

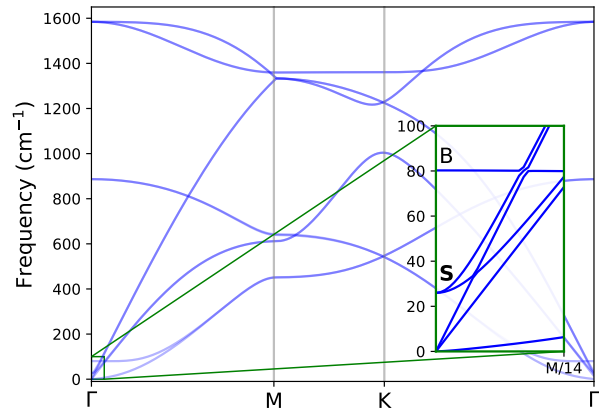


FIG. 3. Bilayer graphene phonon dispersion. The inset shows a zoom in close to Γ to better visualize the doubly degenerate shear modes **S** at Γ , and the breathing mode **B**. Due to the high speed velocity in graphene, the region of the shear mode in the BZ is small (a fraction of ΓM), and is overrepresented in small supercell calculations. The breathing mode, on the other hand, is flat, so nearby sampling points are not necessary to converge the free energy.

In order to compare with our 2-layer calculations, we multiply by a correction factor using a nearest-neighbor model for layers⁴³. In the case of bulk, such a factor is $\sqrt{2}$ (the force exerted by a layer below and above, proportional to the square of the frequency, is doubled when considering only nearest neighbor interactions), which we use to compare to the bulk measurements of Ref. 31. The temperature dependence of both SSCHA and QHA curves is similar to the experimental adjusted bulk values. Folded graphene values have a steeper dependence but are likely unsuitable for comparison, because layers fold with different rotational angles, while layers are aligned in standard graphite. The shear frequency has also been measured in other materials like bilayer NbSe₂ in Ref. 43, or bulk *h*-BN in Ref. 44, which show a similar temperature dependence (adjusting the bulk value by a $\sqrt{2}$ factor) of roughly $-0.5 \text{ cm}^{-1}/100 \text{ K}$.

To further check the adequacy of our method (the use of SSCHA with the in-plane³⁹ and out-of-plane⁴⁰ interatomic potentials), we look at the TE in the previous calculations and also in bulk graphite, and compare to experiments.

In Fig. 5, we show the TE coefficient calculated with SSCHA and QHA in bulk, compared with experimental data^{34,37} and PIMD calculations³⁶. SSCHA results underestimate the thermal expansion. PIMD results are overall very good, although they also give values somewhat lower than experiments^{34,37}.

In-plane SSCHA calculations give excellent results. QHA works well at low temperatures but departs from experiments at higher temperatures. PIMD calculations of Ref. 36, although they work very well out-of-plane,

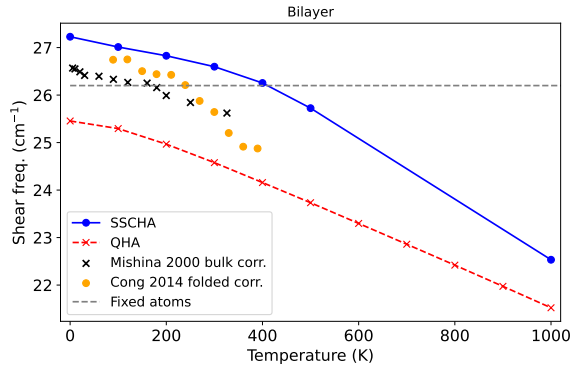
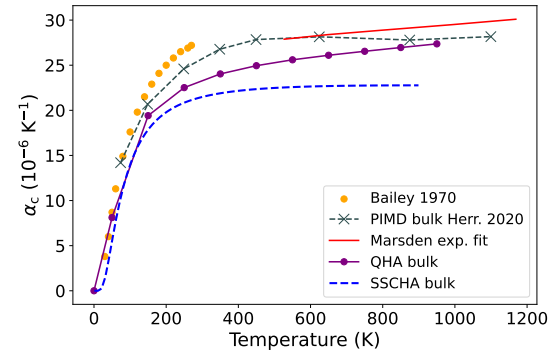


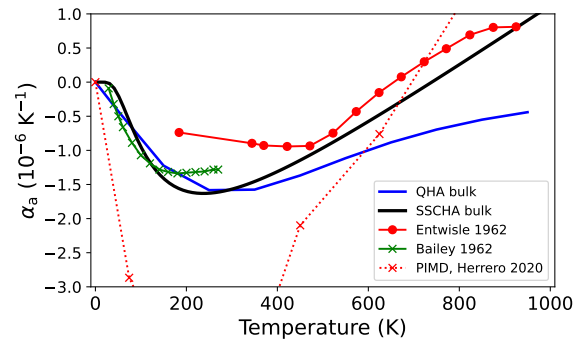
FIG. 4. Shear frequency as a function of temperature using SSCHA (blue circles) and QHA (red crosses). There is no experimental data for the temperature dependence of the shear frequency as a function of temperature for bilayer graphene. Experimental values correspond to bulk (blue crosses) and folded 2+2 graphene (orange circles), which are corrected by the factor of a nearest neighbor model⁴³ to compare to the bilayer case (and rigidly shifted by -5 cm^{-1} to facilitate the visual comparison). The agreement with the temperature dependence of the bulk values is good.

greatly overestimate in-plane TE, presumably due to the inadequacy of their interatomic potential. It would be interesting in future work to compare SSCHA and PIMD using the same potentials.

To conclude, we demonstrated that quantum fluctuations are fundamental to determining properties of layered materials that account for friction. Using the self-consistent harmonic approximation, which can calculate the quantum free energy at unstable configurations, and a novel interpolation method, we unveiled the suppression of the barrier separating stable configurations in bilayer graphene. Quantum fluctuations reduce the free energy barrier by 35%, and gets further reduced at high temperatures. The shear modes, which occupy a small region of phase space, have to be adequately sampled to correctly determine the free energy barrier as well as the thermal expansion. Although our approach underestimates the out-of-plane thermal expansion compared with experimental values, in-plane agreement with experiments is excellent. We also obtained that the temperature dependence of the barrier is similar to that of the shear frequency, which agrees well with existing measurements.



(a)



(b)

FIG. 5. (a) Graphite out-of-plane coefficient of thermal expansion as a function of temperature using SSCHA and QHA. PIMD calculations³⁶ and experimental data³⁴ are also included. PIMD overall agrees well, while QHA and SSCHA (with the potential of Ref. 40) underestimates the TE. (b) Graphite in-plane coefficient of thermal expansion using SSCHA and QHA. QHA again underestimates the dependence at low temperatures, and also at high temperatures. On the other hand, PIMD gives a dependence that is surprisingly very far from experimental values. SSCHA gives excellent results both at low and high temperatures, considering also the disagreement within experimental data.

ACKNOWLEDGMENTS

This work has received funding from the European Union's Horizon 2020 research and innovation programme under Grant Agreement No. 881603, and from the MORE-TEM ERC-SYN project, Grant Agreement No. 951215.

APPENDIX

A1. Calculation details

a. Quasi-harmonic approximation (QHA)

In the QHA, at each value of the lattice parameters $\{a_i\}$, the free energy $F(T, \{a_i\}) = U(\{a_i\}) - TS(T, \{a_i\})$ is given by the standard harmonic expression. That is,

$$F(T, \{a_i\}) = U_{\text{lat}}(\{a_i\}) + \frac{1}{N} \sum_{\mathbf{q}\nu} \frac{1}{2} \hbar \omega_{\mathbf{q}\nu}(\{a_i\}) + \frac{1}{N} \sum_{\mathbf{q}\nu} kT \ln \left(1 - e^{-\hbar \omega_{\mathbf{q}\nu}(\{a_i\})/kT} \right) \quad (\text{A1})$$

The value of the lattice parameters at a given temperature, $a_i(T)$, is determined by minimizing the free energy. Using an interatomic potential, the phonon frequencies at each value of the lattice parameters can be determined with little computational effort, and thus the QHA offers a quick method to determine the lattice expansion. Using first-principles calculations, phonons can be determined using density functional perturbation theory (DFPT), which uses a primitive cell and is much faster than frozen phonon (finite differences) calculations in supercells. However, it does not account for the ‘‘true anharmonicity’’⁴⁵, present at fixed values of the parameters when varying temperature. For example, it gives an increasing as opposed to decreasing temperature dependence of the G mode in graphene, due to the negative TE of the lattice parameter. Also, if the TE is negative and the lattice parameter reduces below the classical lattice value, as in the case of monolayer graphene at about 400 K (see later Fig. A10), then an acoustic mode becomes unstable and the QHA is ill-defined. These issues are not present in SSCHA.

b. Stochastic self-consistent harmonic approximation (SSCHA)

In general, the free-energy of an ionic Hamiltonian $H = T + V$ is given by

$$F_H = \text{tr}(\rho_H H) + \frac{1}{\beta} \text{tr}(\rho_H \ln \rho_H) \quad (\text{A2})$$

where ρ_H is the density matrix. In SSCHA, the density matrix is restricted to a trial harmonic Hamiltonian $\mathcal{H} = T + \mathcal{V}$, and the free energy is given by

$$\mathcal{F}_H(\mathcal{H}) = \text{tr}(\rho_{\mathcal{H}} H) + \frac{1}{\beta} \text{tr}(\rho_{\mathcal{H}} \ln \rho_{\mathcal{H}}) \quad (\text{A3})$$

Due to a variational principle, $F_H \leq \mathcal{F}_H(\mathcal{H})$. The parameters of the harmonic Hamiltonian \mathcal{H} include the centroids of the atoms, which correspond to the lattice parameters a_i of the QHA, but it also includes the interatomic force constant matrix, which contains the information of all the phonon frequencies and accounts for the true anharmonicities. Thus, SSCHA has additional parameters, and is expected in general to give better results than QHA. Also, QHA does not satisfy a variational principle. It can be shown that

$$\mathcal{F}_H(\mathcal{H}) = F_{\mathcal{H}} + \int d\mathbf{R} [V(\mathbf{R}) - \mathcal{V}(\mathbf{R})] \rho_{\mathcal{H}}(\mathbf{R}) \quad (\text{A4})$$

where \mathbf{R} indicates a general ionic configuration and $\rho_{\mathcal{H}}(\mathbf{R}) = \langle \mathbf{R} | e^{-\beta \mathcal{H}} | \mathbf{R} \rangle / Z_{\mathcal{H}}$ is the probability density of finding the crystal in a generic configuration \mathbf{R} ($Z_{\mathcal{H}} = \text{tr}[e^{-\beta \mathcal{H}}]$ the partition function). By stochastically sampling configurations \mathbf{R} for a given density matrix $\rho_{\mathcal{H}}$, and determining the gradient of the free energy with respect to the harmonic parameters (centroids and force constant matrix elements), the free energy can be minimized self-consistently. We used 24000 configurations in all calculations. A detailed description of SSCHA can be found for example in Refs. 46 or 38.

The logarithm term in Eq. A1 can be hard to converge for low frequencies. So rather than calculating $F_{\mathcal{H}}$ directly with the grid corresponding to the SC used in the minimization procedure, the force constant matrix can be Fourier interpolated in the usual way, and $F_{\mathcal{H}}$ can be calculated using a dense grid. This is the novel SSCHA interpolation method we mentioned in the main section, which was used with a 40×40 in-plane grid to determine the barrier and also the out-of-plane TE. To properly determine the barrier, the interpolation scheme is used both at equilibrium and at SP, and then the interpolated free energies are subtracted.

The SSCHA frequencies are in principle auxiliary frequencies that minimize the free energy. In a purely harmonic system, such frequencies correspond to the physical frequencies. But in general, they have to be corrected with the so-called ‘‘bubble correction’’ (and also an additional higher order term in very anharmonic cases)³⁸. Later in Fig. A5, we show the temperature dependence of both the auxiliary and physical frequencies.

A2. Barrier

To determine the barrier, the free energy has to be determined at the equilibrium position and SP. At the equilibrium position, there are two shear modes, indicated with \mathbf{S} in Fig. 3(b). As mentioned in the main text, the mode perpendicular to the bond direction shown in Fig. 1 is stable in SP, while the shear

mode along the reaction coordinate (using the language of chemical reactions) is unstable. As opposed to the breathing mode, that is flat around Γ , the shear modes are only present in a small region of the BZ ($1/N^2$, with N larger than 20), as a result of the large speed of sound in graphene. So in small supercells, the shear modes will be over-represented. This is more problematic at SP, where the SSCHA frequency corresponding to the unstable mode takes very small values (see Fig. A1), which makes the convergence of the free energy hard, mostly due to the logarithm term in $F_{\mathcal{H}}$ in Eq. (A4). Just determining the barrier with this equation and a $N \times N \times 1$ supercell, results in Fig. A2, which is not well converged.

In order to get better convergence, we use the interpolation method we mentioned in Sec. A1 b, and obtain a much more stable barrier as a function of $1/N$ (see Fig. A3). The 40×40 interpolation grid used for $F_{\mathcal{H}}$ corresponds to a supercell of 6400 atoms. For 100, 200 and 300 K, the barrier seems well converged. For a 1000 K, the trend seems to indicate convergence within 0.02 meV/atom, so for the intermediate temperatures 400 and 500 K, the barrier is likely also converged within a similar error, resulting in Fig. 2 of the main text.

To better understand the reduction in the barrier, we show in Fig. A4 the SSCHA frequencies (around the shear modes) at equilibrium and SP at $T = 100$ K. The SSCHA frequencies at equilibrium are similar to the standard harmonic values, as shown in the main text. The SSCHA shear frequencies at SP instead change significantly. The shear mode that looks like an acoustic mode takes a value of about 2 cm^{-1} at Γ (see also Fig. A1). The rest of the SSCHA phonon dispersion presents small differences between equilibrium and SP frequencies.

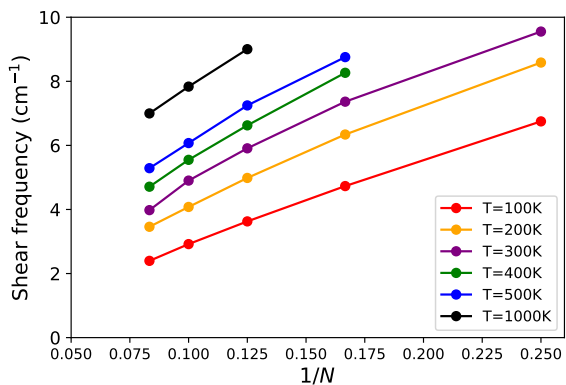


FIG. A1. Unstable shear frequency at SP as a function of $1/N$, for different temperatures. The fact that it does not stabilize shows that the shear mode is present in a small region of the BZ.

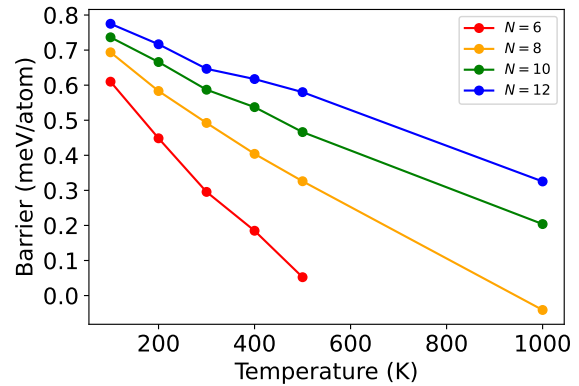


FIG. A2. Barrier as a function of temperature, for different supercells, just using the $N \times N \times 1$ grid to determine the harmonic part of the free energy Eq. (A4). The barrier changes significantly with N , which means the shear mode is over-represented. On the other hand, interpolating the harmonic part of the free energy, convergence is much better. See Fig. A3.

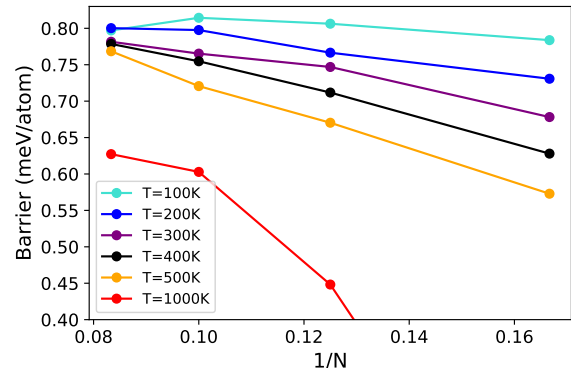


FIG. A3. Barrier as a function of $1/N$, for different temperatures, interpolating the first term of Eq. A4. The barrier seems well converged at low temperatures and harder to converge at higher temperatures. Values are likely converged within less than 0.05 meV/atom.

A3. Shear and breathing frequency

The SSCHA auxiliary and physical frequencies as a function of temperature can be observed in Fig. A5. The frequencies are not fully converged, and the converged value might be similar to the QHA. The bulk temperature dependence (corrected with the factor of the nearest neighbor model) agrees very well with QHA.

The other mode at Γ that involves the layers moving out of phase is the breathing mode (out-of-plane instead of in-plane). Its temperature dependence can be seen in Fig. A6. It decreases more at low temperatures compared to the shear mode and barrier. There are no measurements of the breathing mode as a func-

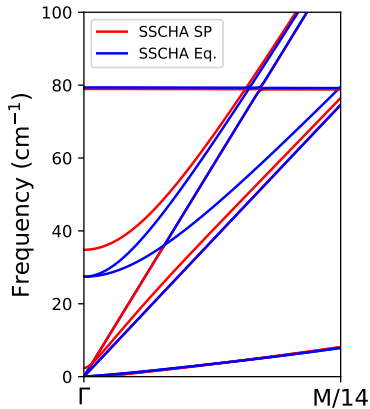


FIG. A4. SSCHA frequencies around the shear modes, at the equilibrium position (blue) and SP (red).

tion of temperature, so our calculations serve as a prediction. The SSCHA curve is very well converged, so we expect it to have a temperature dependence that is closer to the experiment relative to the QHA curve. The auxiliary frequency for $N = 8$ and 10 is almost the same (Fig. A7), so the physical values are also converged (within 0.5 cm^{-1} at 1000 K, and less for lower temperatures).

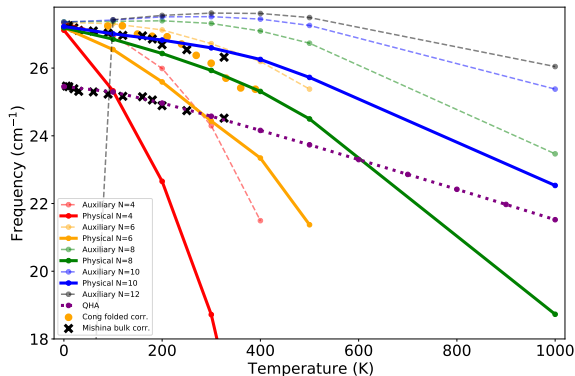


FIG. A5. Shear frequency as a function of temperature, both for the physical frequency (full lines) and the auxiliary one (dashed). The experimental value is shifted and included twice, to facilitate the comparison of the temperature dependence with the QHA and SSCHA curves. The agreement of the experimental bulk value (adjusted with the nearest neighbor model to the bilayer case) with QHA is excellent, and with SSCHA is very good as well.

A4. Thermal expansion (TE)

The interlayer distance and in-plane lattice parameter obtained in bulk with SSCHA can be seen in Fig. A8.

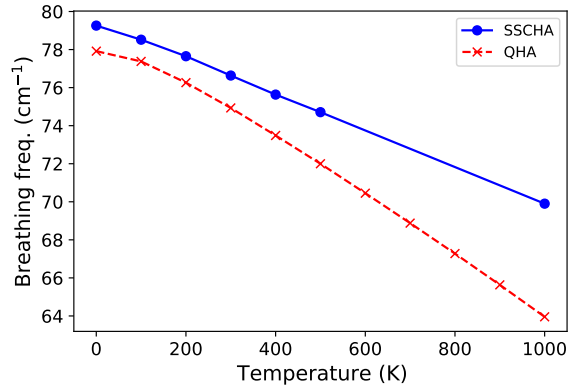


FIG. A6. Breathing frequency as a function of temperature using SSCHA (black circles) and QHA (red crosses). The SSCHA calculations are well converged and serve as a prediction, since there is no experimental data in the literature.

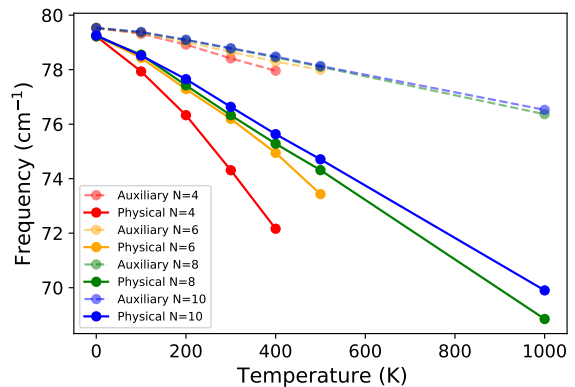


FIG. A7. Convergence of the auxiliary (dashed) and physical (full) breathing frequency. The physical frequency is well-converged at $N = 10$.

The fit corresponds to Eq. (6) of Ref. 47, both for in and out-of-plane TE (b can be a or c_d),

$$b(T) = b_0 \exp\left(\frac{X\theta}{e^{X/T} - 1}\right), \quad (\text{A5})$$

which depends on parameters b_0 , X and θ . In Fig. A9 we compare SSCHA and QHA for bilayer graphene and bulk. The TE for both SSCHA and QHA bulk is lower relative to bilayer. In-plane, Fig. A10, we can also see a clear reduction of the TE coefficient of the TE coefficient from monolayer to bulk. In what follows, we describe in detail convergence studies we did for SSCHA, and also for QHA calculations.

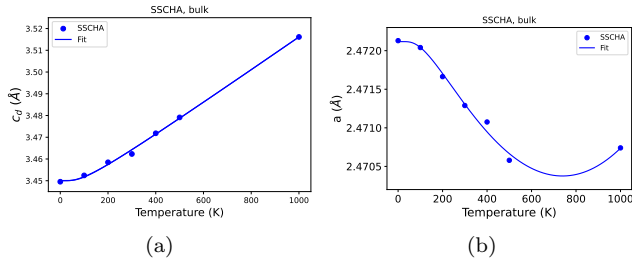


FIG. A8. Out-of plane (a) and in-plane (b) SSCHA thermal expansion (blue dots). The fit corresponds to Eq. (A5).

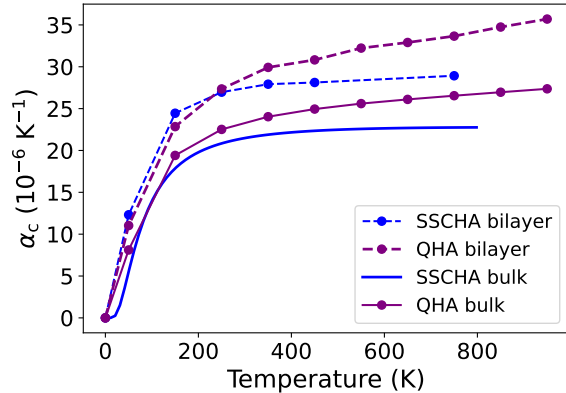


FIG. A9. SSCHA and QHA out-of-plane coefficient of TE for graphite and bilayer graphene.

a. Bilayer

QHA. We first considered the out-of-plane TE by fixing a , and then we considered the full minimization of the free energy by varying both a and c_d . In Fig. A11 we can see $c_d(T)$ both for fixed a , and for the full minimization. The full minimization has a slightly larger dependence with temperature, but fixing a is a good approximation. Fig. A12 is analogous for $a(T)$, with a fixed value $c_d = 3.5 \text{ \AA}$. The curves are very similar, except for a small difference at high temperatures (of about 0.0005 \AA at 1000 K).

We also studied convergence with the size of the grid (Fig. A13). At $N = 12$, $c_d(T)$ is well converged (within 0.005 \AA at 1000 K), although $N \sim 20$ to achieve full convergence. The shear mode increases thermal expansion because when layers are displaced relative to each other, the interlayer distance is larger (see Fig. A14).

In-plane, a larger N of about 50 is needed to fully achieve convergence (A15).

SSCHA. Out-of-plane convergence is similar to the QHA case. So $N = 12$ should give a good curve for $c_d(T)$. We also see in SSCHA a similar variation of c_d when changing a (compare Figs. A11 and A18).

On the other hand, $a(T)$ is already converged at about

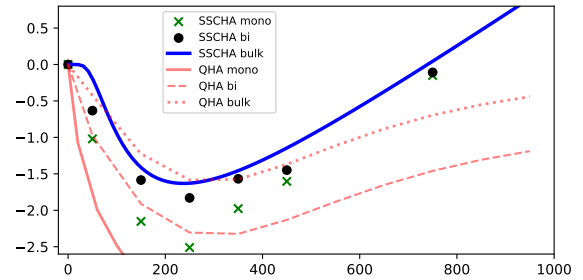


FIG. A10. In-plane coefficient of TE using SSCHA and QHA, for monolayer, bilayer and bulk.

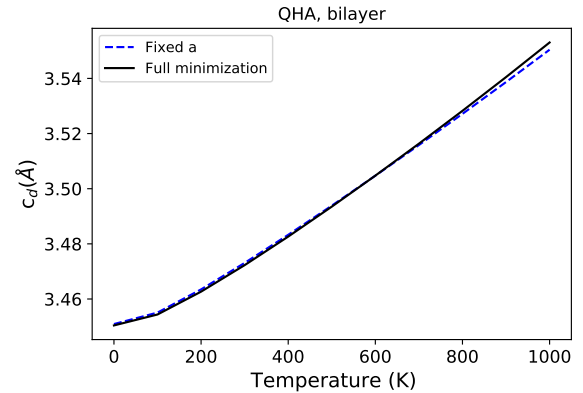


FIG. A11. Interlayer distance c_d as a function of temperature in bilayer graphene using QHA, fixing the value of a (dashed-blue) and doing the full minimization (full-black). In-plane TE has little effect on the out-of-plane TE.

$N = 8$ (Fig. A17).

b. Bulk

QHA. In bulk, there is virtually no difference for the out-of-plane TE when fixing a , or considering also the minimization of a (Fig. A13).

In-plane (Fig. A19), there is a small difference between both fixing or varying a , similar to the bilayer case.

SSCHA. Here we also used the interpolation method (40×40 grid), to go beyond the $N = 8$ supercell that was possible in the direct SSCHA calculation, resulting in the blue dots of Fig. A8 a.

In-plane, based on $N = 8$ already giving converged results in bilayer (Fig. A17), and also considering that the QHA convergence in bulk (Fig. A23) is much faster than in bilayer (Fig. A15), $N = 8$ should give converged SSCHA results in bulk, which corresponds to the blue dots in Fig. A8 b.

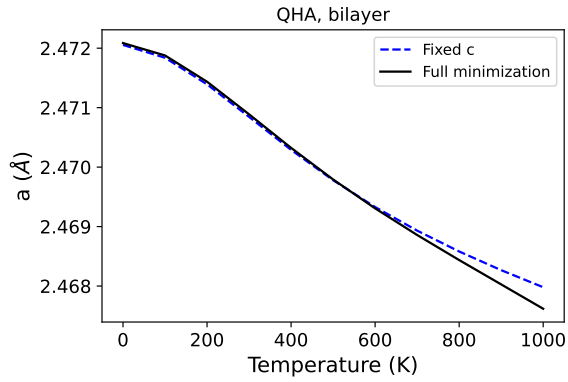


FIG. A12. Lattice parameter a as a function of temperature in bilayer graphene using QHA, fixing the value of c_d (dashed-blue) and doing the full minimization (full-black). In-plane TE has little effect on the out-of-plane TE.

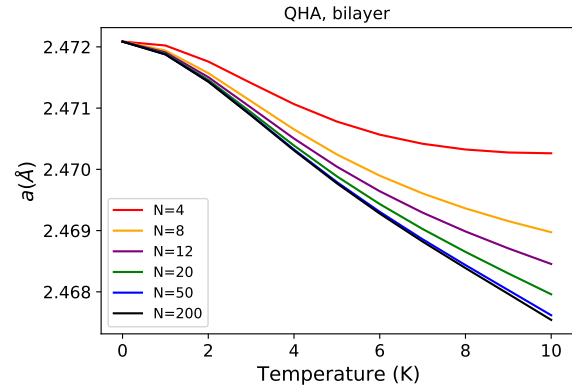


FIG. A15. In-plane lattice parameter as a function of temperature in bilayer graphene for different N using QHA. A large N is needed to achieve convergence.

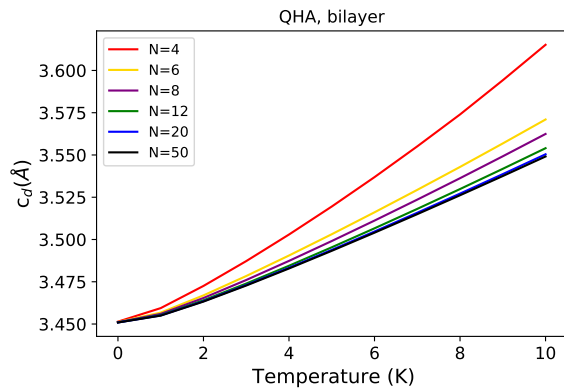


FIG. A13. Interlayer distance as a function of temperature in bilayer graphene, using QHA. At $N \sim 20$ c_d is converged, although $N = 12$ also gives a good result.

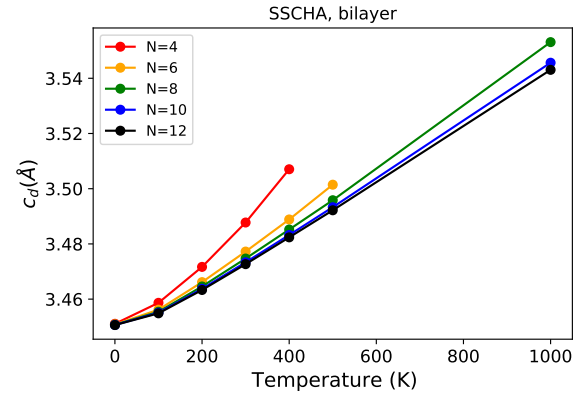


FIG. A16. Interlayer distance as a function of temperature in bilayer graphene for different N using SSCHA. Convergence is similar to the QHA case, Fig. A13, where $N = 12$ gives a good value of $c_d(T)$.

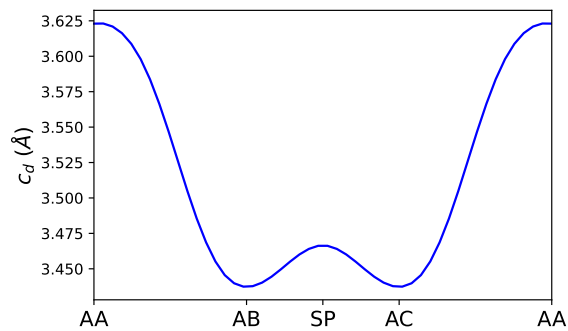


FIG. A14. Interlayer distance profile along the bond direction, when moving a graphene layer relative to another one (analogous to Fig. 1, but for distance instead of energy). The minimum distance is at the equilibrium positions.

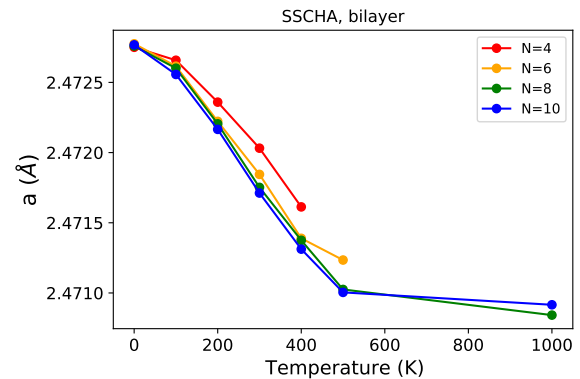


FIG. A17. In-plane lattice parameter as a function of temperature, for different N . At $N = 8$ the curve is already well converged.

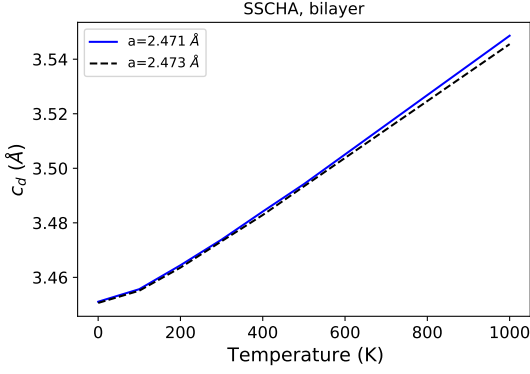


FIG. A18. Interlayer distance as a function of temperature in bilayer graphene, using SSCHA, at two different values of the in-plane lattice parameter. The curves are similar to the ones of Fig. A11. In-plane TE has little effect on the out-of-plane TE.

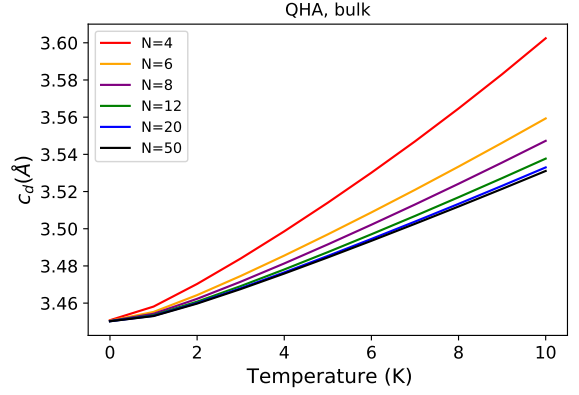


FIG. A21. Interlayer distance as a function of temperature in graphite for different N using QHA. Convergence is similar to the bilayer case.

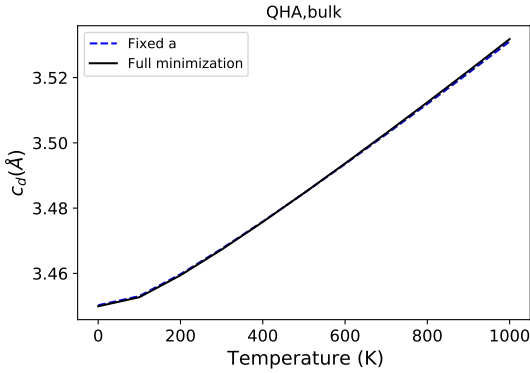


FIG. A19. Interlayer distance as a function of temperature in bulk using QHA, fixing the value of c_d (dashed-blue) and doing the full minimization (full-black). In-plane TE has barely no effect on the out-of-plane TE.

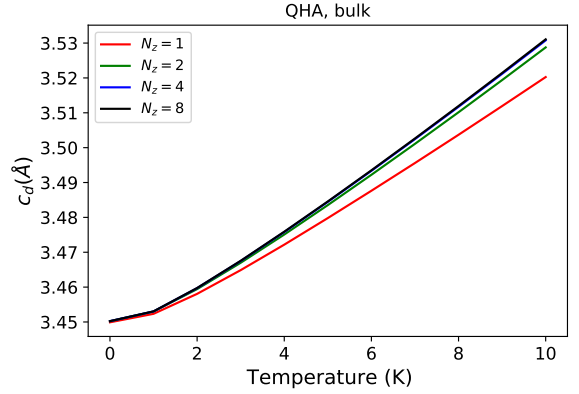


FIG. A22. Interlayer distance as a function of temperature in graphite for different N_z . $N_z = 2$ is the value used in our calculations.

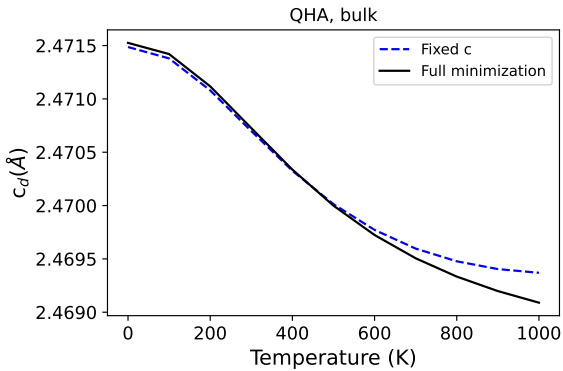


FIG. A20. In-plane lattice parameter as a function of temperature in bulk using QHA, fixing the value of c_d (dashed-blue) and doing the full minimization (full-black). The out-of-plane TE has a slightly larger but similar effect relative to bilayer on the in-plane TE.

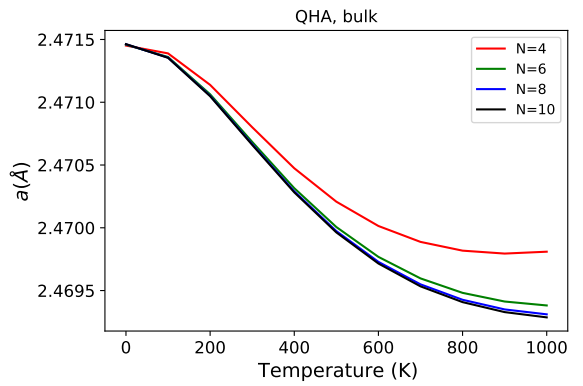


FIG. A23. In-plane lattice parameter as a function of temperature in graphite using QHA, for different N . At $N = 6$ convergence is already very good, as opposed to the bilayer case Fig. A16.

- * nery.jeanpaul@gmail.com
† francesco.mauri@uniroma1.it
- ¹ M. Koshino, *Physical Review B* **81** (2010), 10.1103/physrevb.81.125304.
 - ² H. Zhou, T. Xie, T. Taniguchi, K. Watanabe, and A. F. Young, *Nature* **598**, 434 (2021).
 - ³ M. Yankowitz, J. I.-J. Wang, A. G. Birdwell, Y.-A. Chen, K. Watanabe, T. Taniguchi, P. Jacquod, P. San-Jose, P. Jarillo-Herrero, and B. J. LeRoy, *Nature Materials* **13**, 786 (2014).
 - ⁴ F. R. Geisenhof, F. Winterer, S. Wakolbinger, T. D. Gokus, Y. C. Durmaz, D. Priesack, J. Lenz, F. Keilmann, K. Watanabe, T. Taniguchi, R. Guerrero-Avilés, M. Pelc, A. Ayuela, and R. T. Weitz, *ACS Applied Nano Materials* **2**, 6067 (2019).
 - ⁵ C. Bouhafs, S. Pezzini, N. Mishra, V. Mišević, Y. Niu, C. Struzzi, A. A. Zakharov, S. Forti, and C. Coletti, *arXiv* (2020).
 - ⁶ Z. Gao, S. Wang, J. Berry, Q. Zhang, J. Gebhardt, W. M. Parkin, J. Avila, H. Yi, C. Chen, S. Hurtado-Parra, M. Drndić, A. M. Rappe, D. J. Srolovitz, J. M. Kikkawa, Z. Luo, M. C. Asensio, F. Wang, and A. T. C. Johnson, *Nature Communications* **11** (2020), 10.1038/s41467-019-14022-3.
 - ⁷ H. Li, M. I. B. Utama, S. Wang, W. Zhao, S. Zhao, X. Xiao, Y. Jiang, L. Jiang, T. Taniguchi, K. Watanabe, A. Weber-Bargioni, A. Zettl, and F. Wang, *Nano Letters* **20**, 3106 (2020).
 - ⁸ A. Kerelsky, C. Rubio-Verdú, L. Xian, D. M. Kennes, D. Halbertal, N. Finney, L. Song, S. Turkel, L. Wang, K. Watanabe, T. Taniguchi, J. Hone, C. Dean, D. N. Basov, A. Rubio, and A. N. Pasupathy, *Proceedings of the National Academy of Sciences* **118** (2021), 10.1073/pnas.2017366118.
 - ⁹ J. P. Nery, M. Calandra, and F. Mauri, *Nano Letters* **20**, 5017 (2020).
 - ¹⁰ Q. Lin, T. Li, Z. Liu, Y. Song, L. He, Z. Hu, Q. Guo, and H. Ye, *Carbon* **50**, 2369 (2012).
 - ¹¹ Y. Henni, H. P. O. Collado, K. Nogajewski, M. R. Molas, G. Usaj, C. A. Balseiro, M. Orlita, M. Potemski, and C. Faugeras, *Nano Letters* **16**, 3710 (2016).
 - ¹² H. Henck, J. Avila, Z. B. Aziza, D. Pierucci, J. Baima, B. Pamuk, J. Chaste, D. Utt, M. Bartos, K. Nogajewski, B. A. Piot, M. Orlita, M. Potemski, M. Calandra, M. C. Asensio, F. Mauri, C. Faugeras, and A. Ouerghi, *Physical Review B* **97** (2018), 10.1103/physrevb.97.245421.
 - ¹³ Y. Yang, Y.-C. Zou, C. R. Woods, Y. Shi, J. Yin, S. Xu, S. Ozdemir, T. Taniguchi, K. Watanabe, A. K. Geim, K. S. Novoselov, S. J. Haigh, and A. Mishchenko, *Nano Letters* **19**, 8526 (2019).
 - ¹⁴ Y. Shi, S. Xu, Y. Yang, S. Slizovskiy, S. V. Morozov, S.-K. Son, S. Ozdemir, C. Mullan, J. Barrier, J. Yin, A. I. Berdyugin, B. A. Piot, T. Taniguchi, K. Watanabe, V. I. Fal'ko, K. S. Novoselov, A. K. Geim, and A. Mishchenko, *Nature* **584**, 210 (2020).
 - ¹⁵ Z. Liu, S.-M. Zhang, J.-R. Yang, J. Z. Liu, Y.-L. Yang, and Q.-S. Zheng, *Acta Mechanica Sinica* **28**, 978–982 (2012).
 - ¹⁶ L. Jiang, S. Wang, Z. Shi, C. Jin, M. I. B. Utama, S. Zhao, Y.-R. Shen, H.-J. Gao, G. Zhang, and F. Wang, *Nature Nanotechnology* **13**, 204–208 (2018).
 - ¹⁷ Y. Liu, F. Grey, and Q. Zheng, *Scientific Reports* **4** (2014), 10.1038/srep04875.
 - ¹⁸ R. C. Sinclair, J. L. Suter, and P. V. Coveney, *Advanced Materials* **30**, 1705791 (2018).
 - ¹⁹ G. Mills and H. Jónsson, *Physical Review Letters* **72**, 1124 (1994).
 - ²⁰ A. Poma, M. Monteferrante, S. Bonella, and G. Ciccotti, *Physical Chemistry Chemical Physics* **14**, 15458 (2012).
 - ²¹ E. M. McIntosh, K. T. Wikfeldt, J. Ellis, A. Michaelides, and W. Allison, *The Journal of Physical Chemistry Letters* **4**, 1565 (2013).
 - ²² J. R. Cendagorta, A. Powers, T. J. H. Hele, O. Marsalek, Z. Bačić, and M. E. Tuckerman, *Physical Chemistry Chemical Physics* **18**, 32169 (2016).
 - ²³ I. V. Lebedeva, A. V. Lebedev, A. M. Popov, and A. A. Knizhnik, *Computational Materials Science* **128**, 45 (2017).
 - ²⁴ M. Mohr, J. Maultzsch, E. Dobardžić, S. Reich, I. Milošević, M. Damnjanović, A. Bosak, M. Krisch, and C. Thomsen, *Physical Review B* **76** (2007), 10.1103/physrevb.76.035439.
 - ²⁵ R. Nicklow, N. Wakabayashi, and H. G. Smith, *Physical Review B* **5**, 4951 (1972).
 - ²⁶ P. H. Tan, W. P. Han, W. J. Zhao, Z. H. Wu, K. Chang, H. Wang, Y. F. Wang, N. Bonini, N. Marzari, N. Pugno, G. Savini, A. Lombardo, and A. C. Ferrari, *Nature Materials* **11**, 294 (2012).
 - ²⁷ M. Hanfland, H. Beister, and K. Syassen, *Physical Review B* **39**, 12598 (1989).
 - ²⁸ D. Boschetto, L. Malard, C. H. Lui, K. F. Mak, Z. Li, H. Yan, and T. F. Heinz, *Nano Letters* **13**, 4620 (2013).
 - ²⁹ M. H. S Amelinckx, P Delavignette, *Chem. Phys. Carbon* **1** (1965).
 - ³⁰ C. Cong and T. Yu, *Nature communications* **5**, 1 (2014).
 - ³¹ T. Mishina, K. Nitta, and Y. Masumoto, *Physical Review B* **62**, 2908 (2000).
 - ³² G. A. McQuade, A. S. Plaut, A. Usher, and J. Martin, *Applied Physics Letters* **118**, 203101 (2021).
 - ³³ R. Mittal, M. K. Gupta, B. Singh, S. Mishra, and S. L. Chaplot, *Solid State Communications* , 114324 (2021).
 - ³⁴ A. C. Bailey and B. Yates, *Journal of Applied Physics* **41**, 5088 (1970).
 - ³⁵ W. Morgan, *Carbon* **10**, 73 (1972).
 - ³⁶ C. P. Herrero and R. Ramírez, *Physical Review B* **101**, 035405 (2020).
 - ³⁷ B. Marsden, A. Mummery, and P. Mummery, *Proceedings of the Royal Society A: Mathematical, Physical and Engineering Sciences* **474**, 20180075 (2018).
 - ³⁸ L. Monacelli, R. Bianco, M. Cherubini, M. Calandra, I. Errea, and F. Mauri, *Journal of Physics: Condensed Matter* **33**, 363001 (2021).
 - ³⁹ F. Libbi, N. Bonini, and N. Marzari, *2D Materials* **8**, 015026 (2020).
 - ⁴⁰ M. Wen, S. Carr, S. Fang, E. Kaxiras, and E. B. Tadmor, *Physical Review B* **98** (2018), 10.1103/physrevb.98.235404.
 - ⁴¹ S. Zhou, J. Han, S. Dai, J. Sun, and D. J. Srolovitz, *Phys-*

- ical Review B **92** (2015), 10.1103/physrevb.92.155438.
- ⁴² R. Bianco, I. Errea, L. Paulatto, M. Calandra, and F. Mauri, Phys. Rev. B **96**, 014111 (2017).
- ⁴³ R. He, J. van Baren, J.-A. Yan, X. Xi, Z. Ye, G. Ye, I.-H. Lu, S. M. Leong, and C. H. Lui, 2D Materials **3**, 031008 (2016).
- ⁴⁴ R. Cuscó, J. H. Edgar, S. Liu, G. Cassabois, B. Gil, and L. Artús, Physical Review B **99** (2019), 10.1103/physrevb.99.085428.
- ⁴⁵ P. B. Allen, Modern Physics Letters B **34**, 2050025 (2019).
- ⁴⁶ I. Errea, M. Calandra, and F. Mauri, Physical Review B **89** (2014), 10.1103/physrevb.89.064302.
- ⁴⁷ J. E. Zorzi and C. A. Perottoni, Computational Materials Science **199**, 110719 (2021).